

Compositional variation and thermal annealing effect on optical properties of Se-Te-Sb semiconductor thin films

E. R. SHAABAN*, H. A. ELSHAIKH^a, M. M. SORAYA^a

^aPhysics Department, Faculty of Science, Al-Azhar University, Assuit, 71542, Egypt

^bPhysics Department, Faculty of Science, Aswan University, Aswan, Egypt

Thin films with thickness of about 1040 nm of the semiconducting glasses $\text{Se}_{80-x}\text{Te}_{20}\text{Sb}_x$ with $x = 0, 2, 4, 6, 8,$ and 10 at. % prepared by melt quench technique was evaporated by thermal evaporation onto glass substrates. The optical constant (refractive index, extinction coefficient, and absorption coefficient) of different composition, and annealed films have been studied as a function of photon energy in the wavelength range $400 - 2500$ nm. Analysis of the optical absorption data shows that the rule of non-direct transitions predominates for as prepared Se-Te-Sb, and allowed direct transition for annealed sample. It has been found that the refractive index increase with increasing Sb content in $\text{Se}_{80-x}\text{Te}_{20}\text{Sb}_x$, and decrease with annealing temperature for $\text{Se}_{76}\text{Te}_{20}\text{Sb}_4$ in crystallization region of DSC curve. In terms of Wemple-DiDomenico model, the dispersion of the refractive index is discussed. The results refer to increase the refractive index with increasing Sb contents over the entire spectral range, which is related to the increased polarizability of the larger Sb atoms (atomic radius, 1.53 \AA), in comparison with Se atoms (atomic radius, 1.22 \AA), while the energy gap decreases with increasing Sb contents, which was discussed in terms of the chemical bond approaches.

(Received November 3, 2013; accepted May 7, 2015)

Keywords: Amorphous semiconductors, Thin films, Optical constants, Energy gap, Cohesive energy, Thermal annealing

1. Introduction

Chalcogenide glasses are based on the chalcogen elements S, Se, and Te. These glasses are formed by the addition of other elements such as Ge, As, Sb, Ga, etc. These glasses are low-phonon energy materials, and are generally transparent from the visible up to infrared. Chalcogenide glasses have a great ability for doping by many elements, hence numerous applications in science and technology have been proposed. Their applications as phase change memories (DVDs), x-ray medical image sensors, highly sensitive vidicons, holographic memories, nonlinear devices, solar cells, and ionic devices have been summarized by K. Tanaka and K. Shimakawa [1]. Se-Te glassy alloys have drawn great importance among chalcogenide glasses, because of their higher photosensitivity, greater hardness, higher crystallization temperature, and smaller ageing effects as compared to pure Se glass for better applications [2]. Furthermore, the addition of third element to Se-Te alloys can improve their properties and make them more suitable for various applications. The insertion of Sb to the chalcogenide glasses expands the glass forming area and also creates compositional and configurational disorder in the system [3–5]. Various workers [6–9] have studied the effect of Sb incorporation on the electrical properties of Se-Te alloys. In general, it is observed that the dc conductivity increases, the activation energy for dc conduction decreases, the thermoelectric power decreases, and the photoconductive decay becomes slower on incorporation of Sb to the binary $\text{Se}_{80}\text{Te}_{20}$ alloy. The effects of Sb

additive and thermal annealing on optical properties of Se-Te-Sb glassy thin films were discussed in the present work. Various authors have studied [10–14] the effect of thermal annealing on optical properties of chalcogenide thin films. Thermal processes are known to be important in inducing crystallization in chalcogenide glasses. Recording materials must be stable in the amorphous state at low temperature and have a short crystallization time. The optical storage based on the amorphous–crystalline phase transition utilizes the large optical reflectivity and optical absorption changes obtained in some semiconductors–semimetal thin films by heat treatment or laser irradiation.

In this work we have studied the effect of Sb addition of structure and optical properties of Se-Te-Sb thin films. Also, the present work was undertaken the effect of thermal annealing on the structure, optical properties and energy gap of $\text{Se}_{76}\text{Te}_{20}\text{Sb}_4$ thin films.

The well known Swanepoel's method has been introduced to determine the refractive index and film thickness in the transparent region. The absorption coefficient that is the extinction coefficient k has been determined from transmittance and reflectance spectra at the strong absorption region. Analysis of the optical absorption data shows that the rule of non-direct transitions predominates for as prepared Se-Te-Sb and allowed direct transition for annealed sample. Single-oscillator Wemple-DiDomenico model has been used to discuss the dispersion of the refractive index. The compositional variation of optical band gap with Se-Te-Sb

thin films is discussed in terms of the chemical bond approaches present in the glassy compositions under study.

2. Experimental details

Different compositions of $\text{Se}_{80-x}\text{Te}_{20}\text{Sb}_x$ ($x = 0, 2, 4, 6, 8,$ and 10 at. %) bulk chalcogenide samples were prepared according to the conventional melt-quenched technique. The Se, Te, and Sb elements of high-purity (5N, Aldrich and Sigma chemical company) were weighed according to their atomic percentage and placed together in a pre-cleaned and outgassed silica ampoule, which was evacuated to a pressure of about 10^{-4} Pa and then sealed. The synthesis was performed in a programmable rocking furnace and slowly heated up to approximately 950°C with the temperature ramp about $5^\circ\text{C}/\text{min}$, for about 24 h. During the melt process, the ampoule was inverted at regular time intervals (~ 1 h) so that the amorphous solid will be homogenous and isotropic. After the synthesis, the melt was quenched rapidly in ice water to obtain the Se-Te-Sb glassy alloy. Then the solid was broken along its natural stress line into smaller pieces suitable for grinding. The glassy compositions of $\text{Se}_{80-x}\text{Te}_{20}\text{Sb}_x$ ($x = 0, 2, 4, 6, 8,$ and 10 at.%) thin films were deposited by evaporating the powdered chalcogenide samples from a resistance heating quartz glass crucible onto dried pre-cleaned glass substrates kept at room temperature, using a conventional coating unit (Denton Vacuum DV 502 A). The films were deposited onto glass substrates at a pressure of about 1×10^{-6} Pa. The thicknesses of the as-deposited films studied are mostly greater than 1000 nm in order to avoid the effect of film thickness. During the deposition process, the substrates were kept at room temperature 300 K and the deposition rate was adjusted at $10 \text{ \AA}/\text{sec}$. The substrates were rotated at slow speed 5 Rev/min to obtain a homogenous and smooth film. During evaporation process, the thickness of the produced films was monitored using FTM6 thickness monitor. The elemental composition of the films was analyzed by using energy dispersive X-ray spectrometer unit (EDXS) interfaced with a scanning electron microscope, SEM (JOEL XL) operating an accelerating voltage of 30 kV. The relative error of determining the indicated elements does not exceed 4%.

X-ray powder diffraction (XRD) Philips diffractometry (1710), with $\text{Cu-K}\alpha 1$ radiation ($\lambda = 1.54056 \text{ \AA}$) have been used to examine the structure of the as prepared and annealed $\text{Se}_{80-x}\text{Te}_{20}\text{Sb}_x$ ($x = 0, 2, 4, 6, 8$ and 10 at. %) thin films. The data collection was performed by step scan mode, in a 2θ range between 5° and 80° with step-size of 0.02° and step time of 0.6 seconds. Pure Silicon~ Si 99.9999% was used as an internal standard.

The transmittance (T) and reflectance (R) optical Spectra of the as-deposited and annealed films were performed at room temperature range using UV-VIS-NIR JASCO-670 double beam spectrophotometer. At normal incidence, the transmittance spectra were collected without substrate in the reference beam in the wavelength range

400-2500 nm, while the reflectance spectra was measured using reflection attachment close to normal incidence ($\sim 5^\circ$). In these measurements, the effect of slit correction was eliminated by adjusting spectrophotometer slit width at 8 nm, which is much less than the width of the interference peaks observed at transparency region of the samples under study.

The calorimetric measurements were carried out in a differential scanning calorimeter Shimadzu 50 with an accuracy of ± 0.1 K. The calorimeter was calibrated, for each heating rate, using well-known melting temperatures and melting enthalpies of zinc and indium supplied with the instrument. Twenty mg powdered samples, crimped into aluminium pans, were scanned at heating rate ($\beta = 10$ K/min). The temperatures of the glass transition, T_g , the crystallization extrapolated onset, T_{in} , and the crystallization peak, T_p , were determined with an accuracy of ± 1 K. Films of glassy alloys of $\text{Se}_{76}\text{Te}_{20}\text{Sb}_4$ and $\text{Se}_{72}\text{Te}_{20}\text{Sb}_8$ were annealed for one hour in a vacuum furnace under a vacuum of 10^{-3} Torr with different annealing temperatures 395, 407, and 417 K, respectively, which are in the range of onset crystallization temperature and maximum crystallization temperature of the samples.

3. Basic theoretical considerations

In accordance with Swanepoel's theory [15], transmittance of thin homogeneous film deposited on a thick, finite, transparent substrate is a complex function of the quantities $\alpha, \lambda, n, s,$ and film thickness d :

$$T(\lambda, s, n, d, k) \Big|_{k=0} = \frac{Ax}{B - Cx \cos \varphi + Dx^2} \quad (1)$$

Where, $A = 16n^2s$, $B = (n + 1)^3(n + s^2)$, $C = 2(n^2 - 1)(n^2 - s^2)$, $D = (n - 1)^3(n - s^2)$, $\varphi = 4\pi nd / \lambda$, and x is the absorbance that is given by $x = \exp(-\alpha d)$. Based on the aforementioned theory, Eq. (1) is valid in line with the following conditions: The film under investigation is a homogeneous one of thickness " d ", complex refractive index " $n^* = n - ik$ ", where n is refractive index and k is the extinction coefficient (k relates the absorption coefficient α by the expression " $k = \alpha \lambda / 4\pi$ "). Assuming that s is the refractive index of the substrate with a thickness several order of magnitude larger than d and the refractive index of the surrounding air =1. Taking all the multiple reflections at the three interfaces into account, in the case of $k^2 \ll n^2$, equation (1), can be implemented. Moreover, the values of the transmission at the extremes of the interference fringes can be obtained from Eq. (1) by setting the interference condition $\cos \varphi = 1$ for maxima and $\cos \varphi = -1$ for minima. From these two new formulae, many of the equations that provide the basis of the method in use are easily derived [15].

4. Results and discussion

4.1. Effect of Sb additive on the optical properties of Se-Te semiconducting thin films

4.1.1. Structural properties

The X-ray diffraction patterns of $\text{Se}_{80-x}\text{Te}_{20}\text{Sb}_x$ ($x = 0, 2, 6, \text{ and } 10$ at. %) thin films deposited at ambient temperature are shown in Fig. 1. The absence of any sharp peaks emphasizes the glassy nature of these compositions. For further examination of the patterns, these amorphous samples had two main diffraction humps of the pure $\text{Se}_{80}\text{Te}_{20}$ and doped $\text{Se}_{80-x}\text{Te}_{20}\text{Sb}_x$ ($x = 0, 2, 6, \text{ and } 10$ at. %) thin film samples. The X-ray intensity data were collected in the angular ranges $2\theta = 5\text{-}80$ degrees. The presence of two amorphous humps may be interpreted in terms of finding of two amorphous phases of glass.

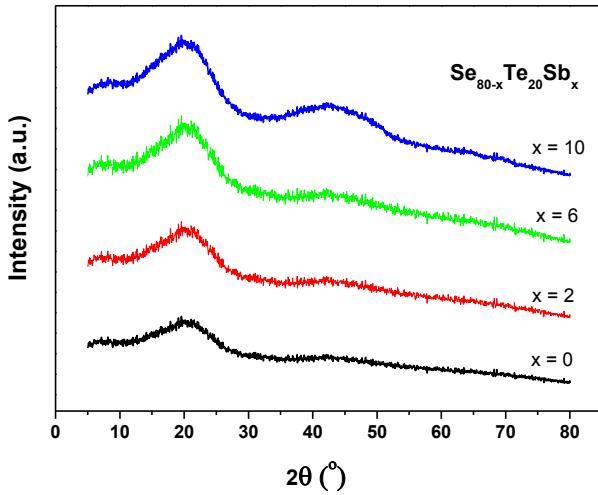


Fig. 1. X-ray diffraction patterns of amorphous $\text{Se}_{80-x}\text{Te}_{20}\text{Sb}_x$ ($x = 0, 2, 6$ and 10 at. %) films prepared by thermal evaporation technique.

4.1.2 Calculation of the refractive index and film thickness

The transmittance, T and reflectance, R spectra of the deposited films as a function of wavelength are illustrated in Fig. 2. It can be seen that the ‘non-shrinking’ interference fringes (fringes of equal chromatic order, FECO) observed in the transmittance spectra at wavelength (800- 2000 nm) indicate the homogeneity and smoothness of the deposited films. Moreover, the absorption edge moves towards the less photon energy as Sb contents increases in the Se-Te glass. This is considered as a result of decreasing the energy gap as Sb substitution for Se atoms in the mentioned Se-Te glass. On the basis of Manifacier et al idea [16] of creating the upper and lower envelopes (Fig. 3a-c) of interference fringes, Swanepoel have introduced a method for analyzing a first, approximate value of the refractive index of the film n_1 , in

the spectral region of medium and weak absorption, according to the expression

$$n = \left[N + (N^2 - s^2)^{1/2} \right]^{1/2} \quad (2)$$

Where

$$N = 2s \frac{T_M - T_m}{T_M T_m} + \frac{s^2 + 1}{2}$$

Here T_M and T_m , are the transmission maximum and the corresponding minimum at a certain wavelength. Alternatively, one of these values is an experimental interference extreme and the other one is derived from the corresponding envelope; both envelopes were computer-generated using the origin version 7 program using more than one procedure. On the other hand, the necessary values of the refractive index of the substrate s are obtained from the transmission spectrum of the substrate, T_s using the well-known Eq. [17]

$$s = \frac{1}{T_s} + \left(\frac{1}{T_s} - 1 \right)^{1/2} \quad (3)$$

The refractive index n , as calculated from Eq. (3) is shown in Table 1. The accuracy of this initial estimation of the refractive index is improved after calculating d , as will be explained below. Now, it is necessary to take into account the basic equation for interference fringes

$$2nd = m\lambda \quad (4)$$

where the order numbers m is integer for maxima and half integer for minima. Moreover, if n_{e1} and n_{e2} are the refractive indices at two adjacent maxima (or minima) at λ_1 and λ_2 , it follows that the film thickness is given by the expression

$$d = \frac{\lambda_1 \lambda_2}{2(\lambda_1 n_{e2} - \lambda_2 n_{e1})} \quad (5)$$

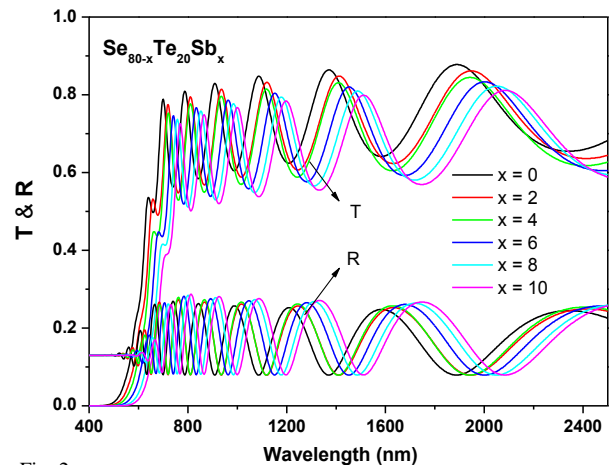


Fig. 2. Optical transmission and reflection spectra of amorphous $\text{Se}_{80-x}\text{Te}_{20}\text{Sb}_x$ ($0 \leq x \leq 10$) deposited on transparent glass substrates by thermal evaporation method.

Table 1. Values of λ , T_M and T_m for the four different composition thin films of amorphous $Se_{80-x}Te_{20}Sb_x$ corresponding to transmission spectra of Fig. 1; the values of transmittance are calculated by origin version 7 program. The calculated values of refractive index and film thickness are based on the envelope method.

Sample	λ	T_M	T_m	s	n_1	$d_1(\text{nm})$	m_0	m	$d_2(\text{nm})$	n_2
Se₈₀Te₂₀										
740	0.7995	0.564	1.5359	2.4872	—	7.051	7	1041.3	2.5164	
786	0.8078	0.573	1.5374	2.4689	1110.5	6.5894	6.5	1034.7	2.4819	
844	0.8166	0.5808	1.5388	2.4568	1044.1	6.1065	6	1030.6	2.4601	
910	0.8245	0.5938	1.5397	2.4226	1021.3	5.5848	5.5	1033	2.4314	
988	0.8342	0.6069	1.54	2.3923	1074.1	5.0795	5	1032.5	2.3998	
1084	0.8442	0.615	1.5394	2.3812	1080.3	4.6082	4.5	1024.3	2.3697	
1210	0.8537	0.6226	1.5372	2.3697	1016.5	4.1085	4	1021.2	2.3512	
1376	0.8625	0.6328	1.5328	2.3458	1009.1	3.5764	3.5	1026.5	2.3396	
1586	0.87	0.6424	1.5264	2.3203	1035.3	3.069	3	1025.3	2.3114	
1882	0.8756	0.6497	1.5201	2.2996	—	2.5633	2.5	1023	2.2857	
$\bar{d}_1 = 1049 \text{ nm} \quad \sigma_1 = 35.9 \text{ nm (3.4 \%)} \quad \bar{d}_2 = 1029 \text{ nm} \quad \sigma_2 = 6.3 \text{ nm (0.61 \%)}$										
Se₇₈Te₂₀Sb₂										
762	0.7861	0.5486	1.5367	2.5251	—	7.0618	7	1056.2	2.5496	
810	0.7934	0.5594	1.5381	2.4959	1094.4	6.5665	6.5	1054.7	2.5166	
868	0.8027	0.5682	1.5392	2.4798	1076.3	6.0882	6	1050.1	2.4894	
938	0.812	0.5793	1.5399	2.4546	1072.3	5.5766	5.5	1050.9	2.466	
1018	0.8212	0.5893	1.5399	2.4337	1114.6	5.0946	5	1045.7	2.433	
1116	0.8302	0.5973	1.539	2.4197	1076.3	4.6206	4.5	1037.7	2.4005	
1248	0.8392	0.6055	1.5363	2.4038	1023.6	4.1046	4	1038.4	2.3861	
1416	0.8471	0.6152	1.5316	2.3785	1026.2	3.5796	3.5	1041.8	2.3689	
1634	0.8537	0.6245	1.525	2.3511	1040.5	3.0662	3	1042.5	2.3431	
1942	0.8584	0.6318	1.5197	2.3288	—	2.5555	2.5	1042.4	2.3206	
$\bar{d}_1 = 1065 \text{ nm} \quad \sigma_1 = 32.6 \text{ nm (3.1 \%)} \quad \bar{d}_2 = 1046 \text{ nm} \quad \sigma_2 = 6.6 \text{ nm (0.63 \%)}$										
Se₇₆Te₂₀Sb₄										
762	0.7619	0.5298	1.5367	2.5562	—	7.0773	7	1043.3	2.5961	
808	0.7705	0.5398	1.538	2.5316	1139.7	6.6099	6.5	1037.3	2.5562	
866	0.7831	0.5477	1.5392	2.5252	1096.8	6.1518	6	1028.8	2.529	
936	0.7955	0.5585	1.5399	2.5059	1050.8	5.6482	5.5	1027.2	2.5056	
1018	0.8062	0.5691	1.5399	2.484	1065.5	5.1479	5	1024.6	2.4774	
1116	0.8148	0.5781	1.539	2.4641	1032.2	4.6581	4.5	1019	2.4443	
1246	0.8202	0.5871	1.5364	2.4367	996.79	4.1259	4	1022.7	2.4258	
1410	0.8251	0.5964	1.5318	2.406	1018.5	3.5999	3.5	1025.6	2.4019	
1626	0.8327	0.6051	1.5253	2.3816	1038.7	3.0901	3	1024.1	2.3742	
1934	0.8435	0.6127	1.5197	2.3691	—	2.5843	2.5	1020.4	2.3533	
$\bar{d}_1 = 1055 \text{ nm} \quad \sigma_1 = 45.6 \text{ nm (4.3 \%)} \quad \bar{d}_2 = 1027 \text{ nm} \quad \sigma_2 = 7.6 \text{ nm (0.74 \%)}$										
Se₇₄Te₂₀Sb₆										
784	0.7548	0.5195	1.5374	2.5886	—	7.0536	7	1060	2.6176	
832	0.7617	0.5294	1.5386	2.5595	1131.5	6.572	6.5	1056.4	2.5795	
892	0.7741	0.5375	1.5395	2.551	1110	6.1096	6	1049	2.5528	
962	0.7858	0.549	1.54	2.5261	1038.4	5.6097	5.5	1047.3	2.5237	
1048	0.7928	0.5603	1.5397	2.4926	1063.7	5.0809	5	1051.1	2.4994	
1148	0.7989	0.5673	1.5384	2.4749	1098.4	4.6055	4.5	1043.7	2.4641	
1282	0.8095	0.5742	1.5355	2.4655	1045.8	4.1085	4	1039.9	2.4459	
1456	0.8201	0.584	1.5304	2.4428	1020.1	3.5841	3.5	1043.1	2.4307	
1682	0.8253	0.5933	1.5238	2.4104	1037.2	3.0614	3	1046.7	2.4068	
2000	0.8285	0.5989	1.5197	2.3913	—	2.5543	2.5	1045.5	2.3849	
$\bar{d}_1 = 1068 \text{ nm} \quad \sigma_1 = 40.3 \text{ nm (3.8 \%)} \quad \bar{d}_2 = 1048 \text{ nm} \quad \sigma_2 = 6.2 \text{ nm (0.59 \%)}$										

Se₇₂Te₂₀Sb₈

852	0.7584	0.5225	1.5389	2.5842	—	6.5151	6.5	1071.5	2.6084
912	0.7672	0.5301	1.5397	2.5695	1114.8	6.0517	6	1064.8	2.5773
984	0.7752	0.5399	1.54	2.5433	1084.2	5.5517	5.5	1064	2.549
1070	0.7843	0.5493	1.5395	2.5212	1102.6	5.0611	5	1061	2.5198
1176	0.7934	0.5569	1.5379	2.5063	1089	4.5777	4.5	1055.8	2.4925
1312	0.8018	0.5644	1.5346	2.489	1046.1	4.0749	4	1054.2	2.4718
1490	0.8092	0.5731	1.5293	2.4633	1034.4	3.551	3.5	1058.6	2.4563
1722	0.8146	0.5814	1.5228	2.4345	1046.7	3.0367	3	1061	2.4332
2052	0.8183	0.5883	1.5201	2.4122	—	2.525	2.5	1063.4	2.4162

$$\bar{d}_1 = 1073 \text{ nm} \quad \sigma_1 = 31.4 \text{ nm (3.2 \%)} \quad \bar{d}_2 = 1062 \text{ nm} \quad \sigma_2 = 5.2 \text{ nm (0.49 \%)}$$

Se₇₂Te₂₀Sb₁₀

926	0.7549	0.5199	1.5399	2.5895	—	5.9805	6	1072.8	2.602
998	0.7671	0.5297	1.54	2.5714	1101.5	5.5102	5.5	1067.3	2.5706
1086	0.7742	0.5391	1.5394	2.544	1083.1	5.0098	5	1067.2	2.543
1194	0.7806	0.5461	1.5375	2.5252	1088.2	4.5229	4.5	1063.9	2.5163
1334	0.7899	0.5529	1.534	2.512	1064	4.0271	4	1062.1	2.4989
1514	0.7988	0.5611	1.5286	2.4905	1043.4	3.5179	3.5	1063.9	2.4816
1752	0.8043	0.5698	1.5221	2.4595	1035.7	3.0023	3	1068.5	2.4615
2088	0.8077	0.5793	1.5206	2.4266	—	2.4855	2.5	1075.6	2.4446

$$\bar{d}_1 = 1069 \text{ nm} \quad \sigma_1 = 26.1 \text{ nm (2.4 \%)} \quad \bar{d}_2 = 1068 \text{ nm} \quad \sigma_2 = 4.6 \text{ nm (0.43 \%)}$$

Table 2. Physical parameters of the constituent elements.

Property	Se	Te	Sb
Energy gap (eV)	1.95	0.65	0.15
Density (g/cc)	4.79	6.24	6.62
Coordination number	2	2	3
Atomic radius (Å)	1.22	1.42	1.53
Electronegativity	2.55	2.1	2.05
Bond energy (Kcal mol ⁻¹)	44.04	33	30.22
Heat of atomization (Kcal mol ⁻¹)	49.4	46	62

The values of d of different samples determined by this equation are listed as d_1 in Table 1. The average value of d_1 (ignoring the last two values), can now be used, along with n_1 , to calculate the “order number” m_0 for the different extremes using Eq. (4). The accuracy of d can now be significantly increased by taking the corresponding exact integer or half integer values of m associated to each extreme (Fig. 3 a-c) and deriving a new thickness, d_2 from Eq. (4), again using the values of n_1 . The values of d found in this way have a smaller dispersion ($\sigma_1 > \sigma_2$). It should

be emphasized that the accuracy of the final thickness is better than 1% (Table 1). With the exact value of m and the very accurate value of Eq. (4) can then be solved for n at each λ and, thus, the final values of the refractive index n_2 are obtained (Table 1). Fig. 4 illustrates the dependence of n on wavelength for different compositions of Se_{80-x}Te₂₀Sb_x ($x = 0, 2, 4, 6, 8, \text{ and } 10$ at. %) chalcogenide glass thin films. Now, the values of n can be fitted to a reasonable dispersion function such as the two-term Cauchy function, $n(\lambda) = B + A/\lambda^2$, which can be used for extrapolation the whole wavelength dependence of refractive index, see Fig. 4. The value of Cauchy coefficient, A and B are listed in Table 3. Fig. 4 shows that the refractive index increases with increasing Sb content, over the entire spectral range studied. This increase is related to the increased polarizability of the larger Sb atoms (atomic radius, 1.53 Å), in comparison with Se atoms (atomic radius, 1.22 Å).

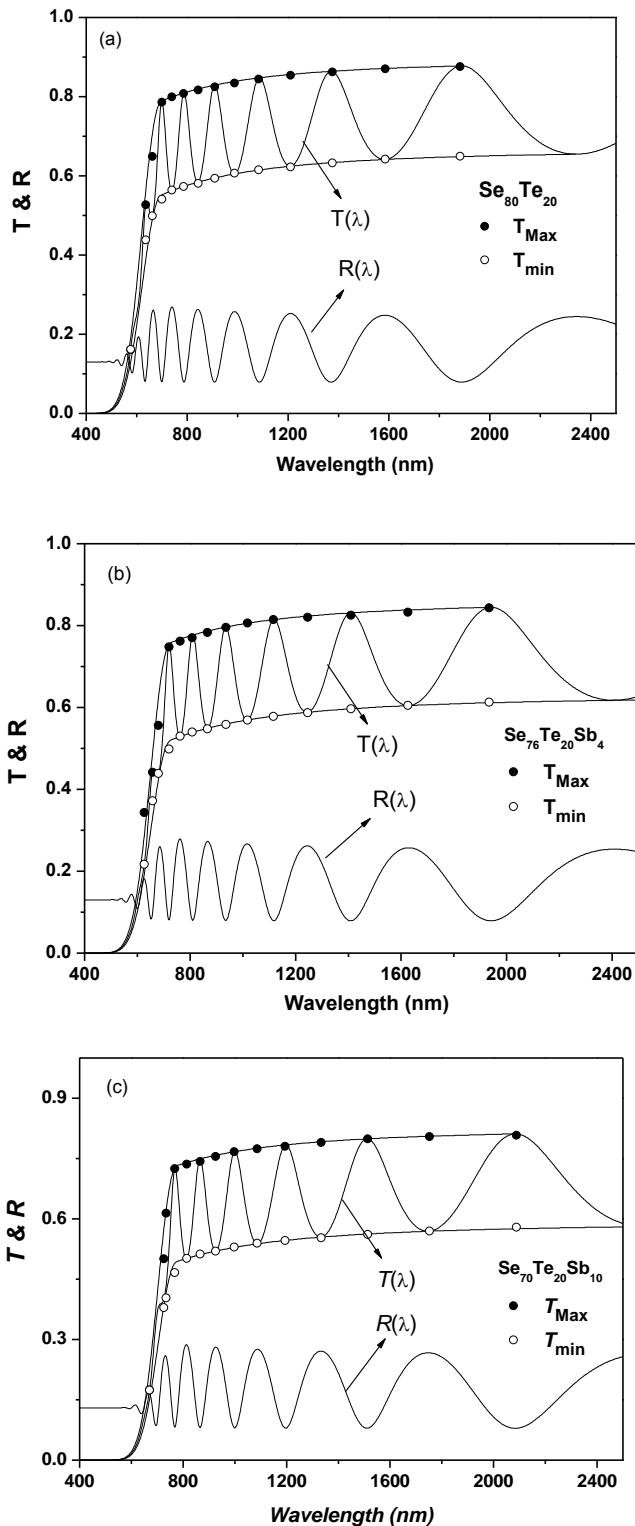


Fig. 3. A typical optical transmission-reflection spectra of (a) $Se_{80}Te_{20}$, (b) $Se_{76}Te_{20}Sb_4$ and (c) $Se_{70}Te_{20}Sb_{10}$ of amorphous thin films deposited using thermal evaporation technique. The top and bottom transmittance envelope T_{max} and T_{min} shown as filled circle and circle, respectively.

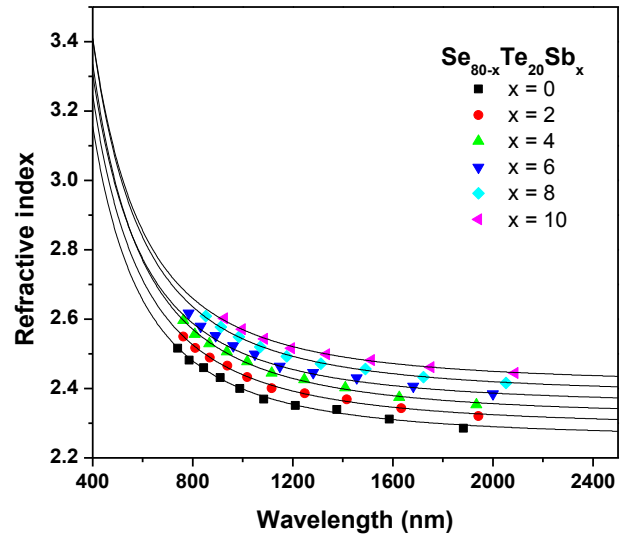


Fig. 4. Dispersion of refractive index of amorphous $Se_{80-x}Te_{20}Sb_x$ ($0 \leq x \leq 10$) thin films obtained from transmission spectra.

The energy dependence of n of amorphous materials can be fitted to the Wemple and DiDomenico dispersion relationship (single-oscillator model) [18] where E_0 is the single-oscillator energy and E_d is the dispersion energy.

$$n^2 - 1 = \frac{E_o E_d}{E_o^2 - (h\nu)^2} \quad (6)$$

By plotting $(n^2 - 1)^{-1}$ versus $h\nu$ and fitting the data to a straight line (as shown in Fig. 5), E_0 and E_d can be determined from the intercept, E_o/E_d and the slope, $-1/E_o E_d$. The values obtained for dispersion parameters E_d and E_0 for six thin film samples are listed in Table 3. Fig. 5 also shows the values of the refractive index $n(0)$ at $h\nu = 0$ for the $Se_{80-x}Te_{20}Sb_x$ ($x = 0, 2, 4, 6, 8$ and 10 at. %) thin films. The obtained values of E_o , E_d and $n(0)$ are listed in Table 3. It was observed that, with increasing Sb content the single-oscillator energy decreases while the dispersion energy and the refractive index $n(0)$ increase. The oscillator energy, E_o is the average energy gap parameter and with a good approximation it varies in proportion to optical band gap ($E_o \approx 2E_g$) [19]. The dispersion energy or single-oscillator strength, E_d , considered as a measure of the strength of interband transitions [20]. E_d increases with increasing Sb content, while there is a decrease in the Se-Te homopolar bonds as shown in table 3. It means antimony is more coordinated in the glass matrix. On the other hand, an important achievement of WDD model is that related to the dispersion energy, E_d , to other physical parameters of material through the following empirical relationship [18]:

$$E_d = \beta N_c Z_a N_e (e\nu) \quad (7)$$

where N_c is the effective coordination number of the cation nearest neighbour to the anion, Z_a the formal chemical valency of the anion, N_e the effective number of valence

electrons per anion and $\beta = 0.37 \pm 0.04$ eV for covalent crystalline and amorphous materials. The value of E_d

increases with increasing Sb content, owing to the increase in the effective coordination of the cation.

Table 3. The fitted Cauchy coefficient, the coordination number N_c , optical bandgap E_g^{opt} , Urbach energy E_e , the single-oscillator energy E_0 , dispersion energy E_d , refractive index $n(o)$ at $(E \rightarrow 0)$, the cohesive energy, the heat of atomization H_s as a function of Sb content of the $Se_{80-x}Te_{20}Sb_x$ thin films.

Sb at. %	Cauchy coefficient		N_c	E_g^{opt} (eV)	E_e (eV)	E_d (eV)	E_0 (eV)	$n(o)$	CE (eV)	Excess of Se-Se bonds	H_s kcal/g/atom	H_s/N_c kcal/g/atom
	B	A $\times 10^5$										
0	2.254	1.444	2.1	1.79	0.0803	14.34	3.486	2.262	1.912	130	48.72	23.200
2	2.286	1.535	2.12	1.75	0.0938	14.62	3.421	2.296	1.931	120	48.972	23.100
4	2.316	1.633	2.14	1.72	0.1118	14.78	3.384	2.317	1.95	110	49.224	23.002
6	2.349	1.533	2.16	1.68	0.1349	15.61	3.372	2.373	1.969	100	49.476	22.906
8	2.379	1.646	2.18	1.64	0.1707	15.72	3.348	2.386	1.988	90	49.728	22.811
10	2.41	1.646	2.2	1.61	0.1908	15.95	3.301	2.415	2.007	80	49.98	22.718

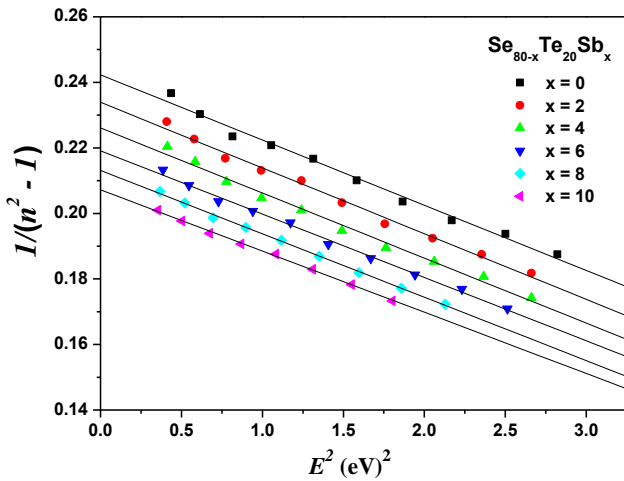


Fig. 5. Plot of refractive index factor $(n^2 - 1)^{-1}$ versus E^2 for $Se_{80-x}Te_{20}Sb_x$ films.

In relevant with the coordination number, the bonding character in the nearest-neighbour region which characterizes the electronic properties of the semiconducting materials. It obeys the so-called 8-N rule, where N is the valency of an atom [21]. According to this rule, the numbers of the nearest-neighbour atoms for Se, Te, and Sb are listed in Table 2. The average coordination number, N_c , of $Se_xTe_ySb_z$ ternary compound ($x + y + z = 1$) can be expressed as [22]:

$$N_c = (xCN(Se) + yCN(Te) + zCN(Sb)) \quad (8)$$

The calculated values of N_c of $Se_{80-x}Te_{20}Sb_x$ ($x = 0, 2, 4, 6, 8$ and 10 at. %) films are listed in Table 3. It can be seen that coordination number increases with increasing the Sb content (as a result of Sb additive to Se-Te matrix).

4.1.3. Determination of the extinction coefficient and optical band gap

The spectral dependence of the optical transmittance (T) and the reflectance (R) of the investigated sample can be obtained using a double-beam spectrophotometer. The absorption coefficient α can be obtained in the strong absorption region of the experimentally measured values of R and T according to the following expression [23]:

$$\alpha = \frac{1}{d} \ln \left[\frac{(1-R)^2 + [(1-R)^4 + 4R^2T^2]^{1/2}}{2T} \right] \quad (9)$$

Where d is the sample thickness. The absorption coefficient as a function of photon energy for the different compositions of is illustrated in Fig. 7. It is clear that the absorption edge ($\alpha \geq 10^4$) shifts towards the less photon energy with increasing Sb contents in all the specimens under study that is related to the decreasing of the optical band gap with the variation of the different chemical compositions as a result of Sb additive. It is convenient now to calculate the extinction coefficient from the values of λ and α using the formula $k = \alpha\lambda/4\pi$. Fig. 6 illustrates the dependence of k on the wavelength for different thin films of $Se_{80-x}Te_{20}Sb_x$ ($x = 0, 2, 4, 6, 8$ and 10 at. %) glasses.

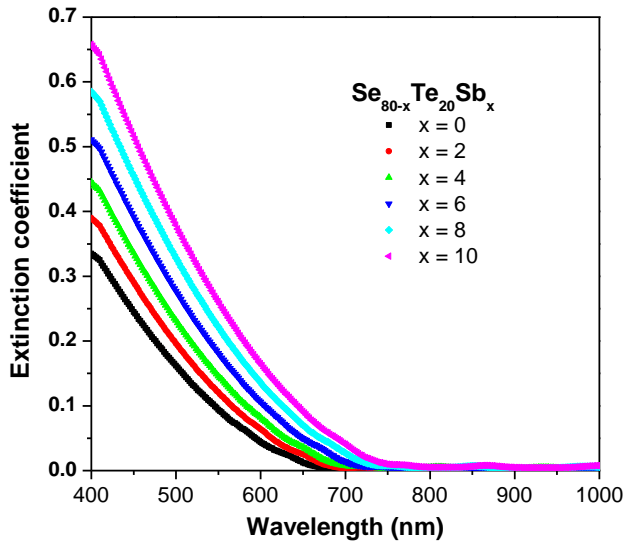


Fig. 6. The extinction coefficient, k versus wavelength, λ for $Se_{80-x}Te_{20}Sb_x$ amorphous thin films.

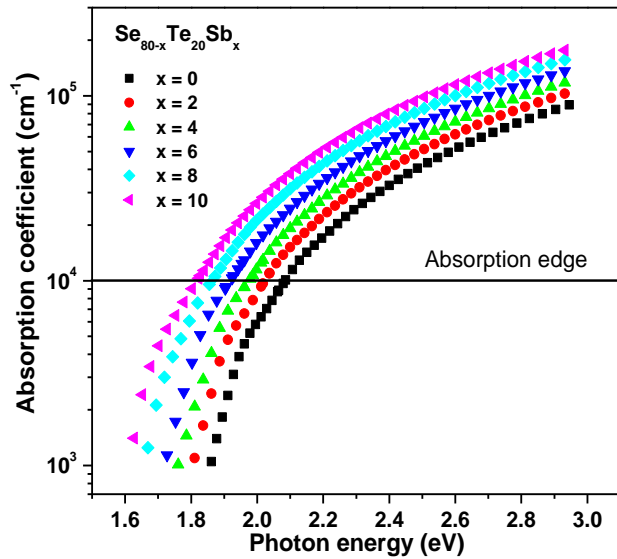


Fig. 7. The absorption coefficient α versus photon energy $h\nu$ for the four samples of $Se_{80-x}Te_{20}Sb_x$ ($x = 0, 2, 4, 6, 8$ and 10 at. %) amorphous films.

It should be pointed out that the absorption coefficient of amorphous semiconductors, in the high-absorption region ($\alpha \geq 10^4$), is given according to Tauc's relation for the allowed non-direct transition [24] by the following equation:

$$\alpha(h\nu) = \frac{K(h\nu - E_g^{opt})^2}{h\nu} \quad (10)$$

Where K is a constant which depends on the transition probability and is E_g^{opt} the optical band gap. Fig. 8 shows a good fitting of $(\alpha h\nu)^{1/2}$ versus photon energy ($h\nu$) for six

different composition thin films. The values of the optical band gap E_g^{opt} were taken as the intercept of $(\alpha h\nu)^{1/2}$ versus $(h\nu)$ at $(\alpha h\nu)^{1/2} = 0$ according to Tauc's relation for the allowed non-direct transition. The optical band gap derived for each film is listed in Table 3.

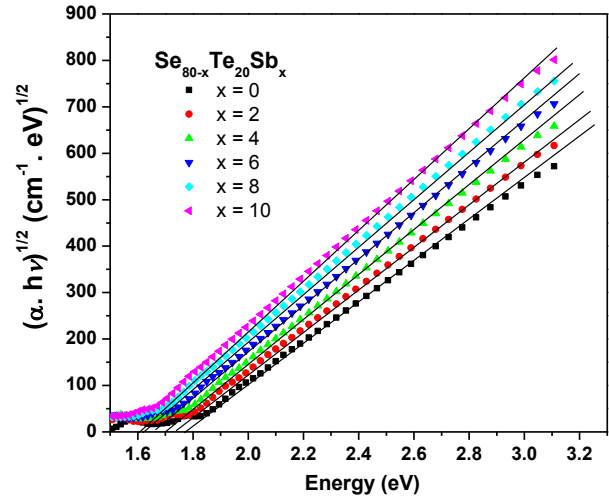


Fig. 8. The dependence of $(\alpha h\nu)^{1/2}$ on photon energy $h\nu$ for the different composition of amorphous $Se_{80-x}Te_{20}Sb_x$ amorphous films, from which the optical band gap E_g^{opt} is estimated (Tauc's extrapolation).

At lower values of the absorption coefficient ($1 \leq \alpha \leq 10^4 \text{ cm}^{-1}$), the absorption depends exponentially on the photon energy (the so-called Urbach relation [25])

$$\alpha(h\nu) = \alpha_0 \exp\left(\frac{h\nu}{E_e}\right) \quad (11)$$

Where α_0 is a constant and E_e is the Urbach energy (related to the width of the band tail of the localized states at the conduction or valence band edge). Fig. 9 shows the dependence of $\ln(\alpha)$ on photon energy $h\nu$ for the different composition of amorphous $Se_{80-x}Te_{20}Sb_x$ amorphous films, from which the Urbach energy E_e is estimated. The values of E_e (the Urbach energy) for the different composition thin films are calculated and listed in Table 3. It is obvious that Energy gap E_g^{opt} decreases with increasing Sb content but the Urbach energy E_e do the opposite (it will be explained latter).

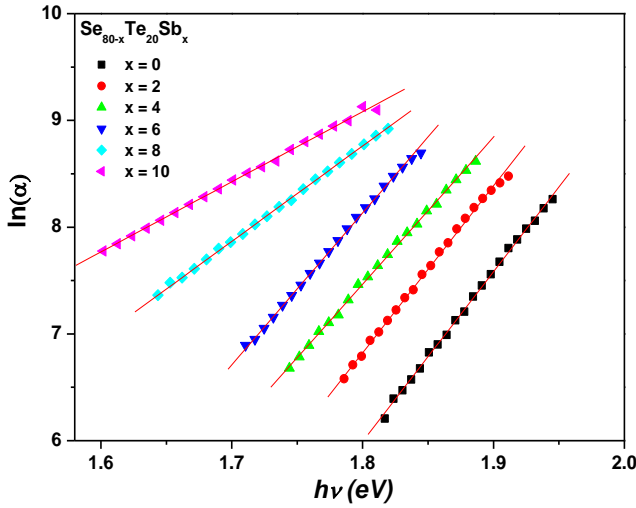


Fig. 9. The dependence of $\ln(\alpha)$ on photon energy $h\nu$ for the different composition of amorphous $Se_{80-x}Te_{20}Sb_x$ amorphous films, from which the Urbach energy E_e is estimated.

In view of the chemical bond approach to examine the structure and properties of various types of chalcogenide glasses, atoms combine more favourably with atoms of different kinds than with the same kind; this assumption which is generally found to be valid for glass structures, has been used by Zachariasen [26] in his covalently bonded continuous random net work model. On using this assumption, bonds between like atoms will only occur if there is an excess of a certain type of atoms. Bonds are formed in the sequence of decreasing bond energies until all available valences for the atoms are saturated. The bond energies $D(A-B)$ for heteronuclear bonds have been calculated by using the relation [21]

$$D(A-B) = [D(A-A) \times D(B-B)]^{1/2} + 30(\chi_A - \chi_B)^2 \quad (12)$$

Where $D(A-A)$ and $D(B-B)$ are the energies of the homonuclear bonds, χ_A and χ_B are electronegativity values for atoms involved. Both the electronegativity and the homonuclear bonds $D(A-A)$ and $D(B-B)$ for Te, Se and Sb are listed in Table 1. The types of bonds expected to occur in the system under investigation are Se-Te bonds (44.2 kcal/mol), Se-Sb (43.98 kcal/mol) and Se-Se (44.04 kcal/mol). In the present compositions the Se atoms strongly bond to Te. The Se-Te bonds have the highest probability to form, then the Se-Sb bonds. After these bonds are formed, there are still unsatisfied Se valences, which are much satisfied by the formation of Se-Se bond. The number of excess Se-Se homopolar bonds for each composition of the $Se_{80-x}Te_{20}Sb_x$ ($x = 0, 2, 4, 6, 8$ and 10 at. %) are listed in Table 3. Knowing the bond energies, the cohesive energy (CE) have been derived by assuming the bond energies over all the bond expected in the system under test by the following equation

$$CE = \sum C_i D_i / 100 \quad (13)$$

Where C_i and D_i are the number of expected chemical bonds and the energy of each corresponding bond. The results of CE are listed in Table 3. It should be mentioned that the approach of the chemical bond neglects dangling bond and other valence defects as a first approximation. Also van der Waals interactions are neglected, which can provide a means for further stabilization by the formation of much weaker links than regular covalent bonds.

In order to complete the vision of the chemical bonds, it is appropriate to obtain the average heat of atomization H_s , which is defined as a direct measure of cohesive energy and considered as the average bond strength. For a compound $A_\alpha B_\beta C_\gamma$, it can be calculated, in kcal/g/atom as the formula [27].

$$H_s = \frac{\alpha H_s^A + \beta H_s^B + \gamma H_s^C}{\alpha + \beta + \gamma} \quad (14)$$

where H_s^A , H_s^B , H_s^C are the heat of atomization of the involved elements (Se, Te, Sb) as shown Table 2 and α , β , γ are the ratios of these elements in the chalcogenide glass system, respectively. The values of H_s for the Se-Te-Sb glass thin films are shown in Table 3, hence another factor serves in understanding the variation of energy gap, H_s/N_c ; the average single bond energy, which specify the bond strength (where H_s is the average heat of atomization and N_c is the average coordination numbers), also calculated and listed in Table 3. These results shows that the average heat of atomization H_s and cohesive energy, which considered as a measure of the average bond strength increase with increasing Sb contents. These results may due to that the decreasing of the relative atomic mass of chalcogen (Se) or its proportion in a given chalcogenide glass system, increases the average bond strength [27, 28] (the increasing of Sb content means a decrease of Se in our chalcogenide glass system, in which the Se atoms replaced by Sb atoms in the Se-Te glass system).

In another manner, the decrease of the energy band with increasing Sb contents can be discussed in three conditions; (1) the average single bond energy; H_s/N_c , which specify the bond strength Shows a decrease with increasing the Sb content (as shown in Table 3) within the glassy composition, resulting in the decrease of the energy gap. This trend of the decrease of H_s/N_c ; the average single bond energy whereas the average heat of atomization H_s and the average coordination number N_c increase, have been denoted earlier by Kawamoto [29] in the As-S binary system and by S.S Fouad et al [30] in Sb_xSe_{1-x} system (2) in view of Urbach energy (the band tail width) as listed in Table 3. It is clear that the E_e increases with increasing Sb content in the chalcogenide glass system, while the energy gap E_g^{opt} decreases, this mean that an additional of Sb lead to an increase of the localized states within the band gap. Davis and Mott [31] reported that the presence of high density of localized state in the band structure is responsible for the lower values of optical gap. It seems

that our results have a good agreement with Davis and Mott suggestion (3) In connection with the last condition, this decrease in optical band gap may be correlated with the electronegativity difference of the elements involved. According to Kastner et al [32], the valence band in chalcogenide glasses is constituted by lone pair p-orbital's contributed by the chalcogen atoms. These lone pair electrons will have a higher value of energies than those of electronegative atoms and adjacent to electropositive atoms, subsequently by the addition of electropositive elements to the alloy, the energy of the lone pair gets enhanced and the valence band moves toward the energy gap. As shown in Table 3, the values of band gaps decreases from 1.79 to 1.61 eV as the Sb content is increased from 0 to 10 at. % in the Se-Te glassy thin films under study. This trend of decreasing the band gap and increasing the band tail width with increasing Sb contents in Se-Te glassy thin films have been denoted by Soltan et al [33] in $\text{Se}_{85-x}\text{Te}_{15}\text{Sb}_x$ chalcogenide glass thin films ($x = 0, 3, 6$ and 9 at.%) with a good agreement of our results.

4.2. Thermal annealing effect on structure and optical constants of Se-Te-Sb in terms of DSC curve

Fig. 10 shows the DSC thermograms for amorphous $\text{Se}_{76}\text{Te}_{20}\text{Sb}_4$ glass recorded at different heating rate 10 K/min. The characteristic feature of this thermogram is the homogeneity of the glass being considered, which is confirmed by the appearance of a small single endothermic peak. This peak is attributed to the glass transition temperature T_g , which represents the strength or rigidity of the glass structure. Also, there is an exothermic peak originating from the amorphous-crystalline transformation. The exothermic peak has two characteristic points: the first point is the onset temperature of crystallization T_{in} and the second is the peak temperature of crystallization T_p . This figure also shows the characteristic melting temperatures, T_m .

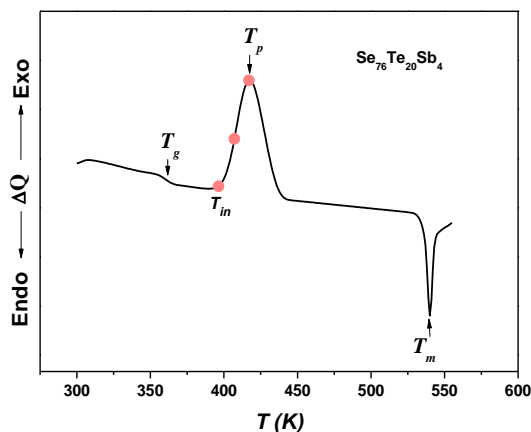


Fig. 10. DSC curve of $\text{Se}_{76}\text{Te}_{20}\text{Sb}_4$ demonstrating the onset and the peak temperature of crystallization.

To identify the possible phases that crystallize during the thermal treatment applied to the samples, the X-ray diffraction patterns of $\text{Se}_{76}\text{Te}_{20}\text{Sb}_4$ thin film annealed at three different annealing temperatures 395, 407 and 417 K, respectively, with a heating rate of 10 K/min for 1h which are in the range of onset crystallization temperature and maximum crystallization temperature of the samples as deduced from non isothermal DSC traces (shown in Fig. 10). The diffractogram of the transformed material after the crystallization process suggests the presence of microcrystallites of main phase of Sb_2TeSe_2 and small traces of Sb and Se as shown in Fig. 11. From the JCPDS files these peaks can be identified as, **1-** Antimony Tellurium Selenide, Sb_2TeSe_2 (40-1211), which crystallizes in the rhombohedral system with lattice parameters $a = b = 0.4121$ nm, $c = 2.9549$ nm, **2-** Antimony, Sb (card No. 5-0562), which crystallizes in the rhombohedral structure with lattice parameters $a = b = 0.4307$ nm and $c = 1.1273$ nm, and **3-** Selenium, Se (card No. 1-0848), which crystallizes in the Hexagonal structure with lattice parameters $a = b = 0.434$ nm and $c = 0.495$ nm.

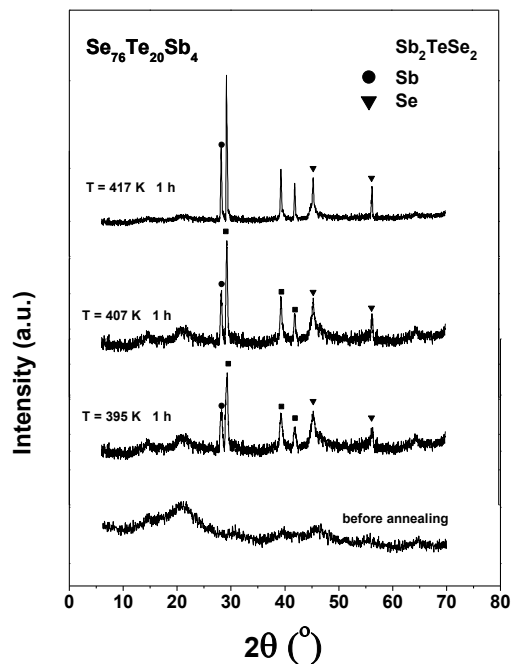


Fig. 11. X-ray diffraction pattern of the as deposited and annealed films of $\text{Se}_{76}\text{Te}_{20}\text{Sb}_4$ at different temperature (395, 407, and 417 K).

Fig. 12 shows the optical transmission and reflection spectra as a function of wavelength of the as prepared and annealed $\text{Se}_{76}\text{Te}_{20}\text{Sb}_4$ films at different temperatures (395, 407, and 417 K). The optical transmission increases with increasing annealing temperature. Both the maximum and minimum of transmission peaks are shifted to the lower wavelength. The film thickness and the refractive index were determined using the same procedures of Swanepoel method for as prepared and annealed $\text{Se}_{76}\text{Te}_{20}\text{Sb}_4$ films at 395, 407 and 417 K, as shown in Table 4, by plotting the

refractive index of the as deposited and annealed samples at different temperatures as function of wavelength as shown in Fig. 13. The values of n were fitted to the two-term Cauchy dispersion function, $n(\lambda) = B + A/\lambda^2$, which can be used for extrapolation the whole wavelength dependence of refractive index as demonstrated in Fig. 13. The value of Cauchy coefficient, A and B are listed in Table 5. From Fig. 13 the refractive index, n decreases with increasing annealing temperature, which can be explained as, chalcogenide thin films always contain a

high concentration of unsaturated bonds or defects. During thermal annealing at temperature below and at the crystallization temperature, the unsaturated defects are gradually annealed out producing a large number of saturated bonds. The reduction in the number of unsaturated defects decreases the density of localized states in the band structure consequently decreasing the refractive index.

Table 4. Values of λ , T_M and T_m for as prepared and annealed $Se_{76}Te_{20}Sb_4$ films at various temperatures (395, 407 and 417 K), corresponding to transmission spectra of Fig. 12; the values of transmittance are calculated by origin version 7 program. The calculated values of refractive index and film thickness are based on the envelope method.

Sample	λ	T_M	T_m	s	n_1	$d_1(\text{nm})$	m_0	m	$d_2(\text{nm})$	n_2
Se₇₆Te₂₀Sb₄										
T = 395 K										
	752	0.7791	0.5411	1.5363	2.5426	—	7.1056	7	1035.2	2.5675
	800	0.7873	0.5538	1.5378	2.5065	1071.3	6.5846	6.5	1037.3	2.5363
	856	0.7992	0.5628	1.539	2.4947	1099.9	6.1248	6	1029.4	2.5051
	922	0.8066	0.5728	1.5398	2.4696	1061.9	5.6293	5.5	1026.7	2.4734
	1002	0.815	0.5824	1.54	2.4484	1042.2	5.1353	5	1023.1	2.4436
	1102	0.8229	0.5927	1.5392	2.4231	1018.5	4.621	4.5	1023.3	2.4188
	1228	0.8304	0.6026	1.5368	2.3978	1037.4	4.1036	4	1024.3	2.3958
	1386	0.8379	0.6103	1.5325	2.3795	1044.2	3.6081	3.5	1019.3	2.3661
	1604	0.8468	0.6175	1.5259	2.3639	1030.9	3.0973	3	1017.8	2.3471
	1908	0.8567	0.6249	1.5198	2.3503	—	2.5888	2.5	1014.8	2.3266
	$\bar{d}_1 = 1051 \text{ nm} \quad \sigma_1 = 25.9 \text{ nm (2.5 \%)} \quad \bar{d}_2 = 1025 \text{ nm} \quad \sigma_2 = 7.2 \text{ nm (0.70 \%)}$									
T = 407 K										
	740	0.7884	0.5518	1.5359	2.5154	—	7.037	7	1029.6	2.5386
	786	0.7966	0.5604	1.5374	2.4977	1074.8	6.5785	6.5	1022.7	2.5038
	844	0.8062	0.5707	1.5388	2.4763	997.16	6.074	6	1022.5	2.4818
	912	0.8153	0.5844	1.5397	2.4408	1014.9	5.5405	5.5	1027.5	2.4583
	988	0.8251	0.5969	1.54	2.4121	1084.5	5.0542	5	1024	2.421
	1084	0.8353	0.6049	1.5394	2.4014	1070.7	4.586	4.5	1015.7	2.3906
	1210	0.8446	0.6125	1.5372	2.3891	1010.9	4.0875	4	1012.9	2.372
	1374	0.8532	0.6227	1.5329	2.3642	1002.7	3.5621	3.5	1017	2.3568
	1584	0.8609	0.6325	1.5265	2.3377	1024.9	3.0552	3	1016.4	2.3289
	1880	0.8671	0.6398	1.5201	2.3177	—	2.5521	2.5	1013.9	2.3034
	$\bar{d}_1 = 1035 \text{ nm} \quad \sigma_1 = 35.6 \text{ nm (3.4 \%)} \quad \bar{d}_2 = 1020 \text{ nm} \quad \sigma_2 = 5.8 \text{ nm (0.57 \%)}$									
T = 417K										
	730	0.7967	0.5648	1.5355	2.4777	—	7.0918	7	1031.2	2.5145
	776	0.8033	0.5747	1.5371	2.4524	1096.4	6.6033	6.5	1028.4	2.482
	830	0.816	0.585	1.5385	2.4387	1120.5	6.139	6	1021.1	2.4505
	894	0.83	0.5956	1.5396	2.4264	1061.9	5.671	5.5	1013.2	2.4195
	974	0.8397	0.6069	1.54	2.4031	1026.9	5.1552	5	1013.3	2.3964
	1068	0.8481	0.6178	1.5396	2.3787	1020	4.6536	4.5	1010.2	2.3649
	1192	0.8583	0.6288	1.5376	2.3567	1009.2	4.1309	4	1011.6	2.3462
	1350	0.8674	0.6379	1.5336	2.3379	1011.2	3.6184	3.5	1010.5	2.325
	1562	0.8739	0.646	1.5271	2.3159	1011.5	3.0978	3	1011.7	2.3058
	1852	0.878	0.6534	1.5204	2.2918	—	2.5856	2.5	1010.1	2.2783
	$\bar{d}_1 = 1045 \text{ nm} \quad \sigma_1 = 43.3 \text{ nm (4.1 \%)} \quad \bar{d}_2 = 1016 \text{ nm} \quad \sigma_2 = 7.9 \text{ nm (0.78 \%)}$									

Table 5. The fitted Cauchy coefficient, optical band gap E_g^{opt} , the single-oscillator energy E_0 dispersion energy E_d , refractive index $n(o)$ at $(E \rightarrow 0)$ as a function of annealing temperature of the $Se_{76}Te_{20}Sb_4$ thin films.

T (K)	Cauchy coefficient		E_g^{opt} (eV)	E_d (eV)	E_0 (eV)	$n(o)$
	B	A x10 ⁵				
RT	2.316	1.633	1.72	14.78	3.384	2.317
395	2.285	1.609	1.82	14.52	3.443	2.284
407	2.27	1.486	1.91	14.40	3.472	2.269
417	2.242	1.443	2.02	14.05	3.558	2.225

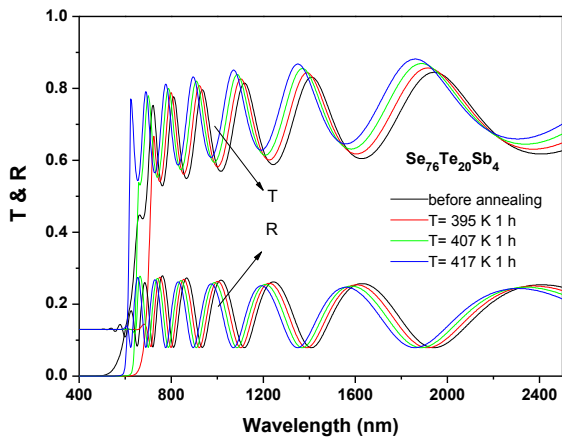


Fig. 12. Optical transmission and reflection spectra of the as prepared and annealed $Se_{76}Te_{20}Sb_4$ films at different temperatures (395, 407, and 417 K).

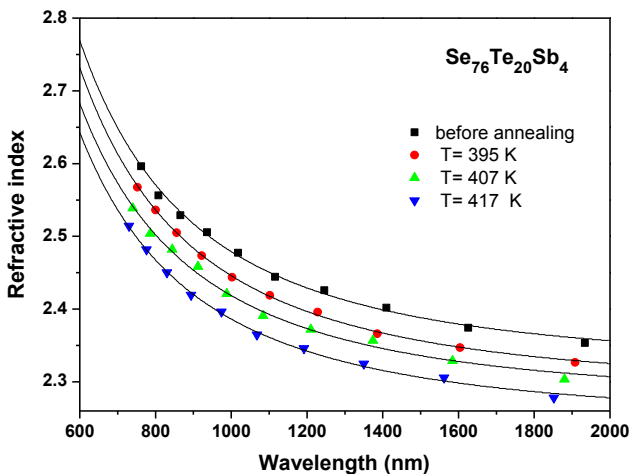


Fig. 13. Dispersion of refractive index of the as prepared and annealed $Se_{76}Te_{20}Sb_4$ films at various temperatures (395, 407, and 417 K).

According to equation (6), a good fitting of the WDD single oscillator dispersion model for the as deposited $Se_{76}Te_{20}Sb_4$ sample and annealed at the last mentioned temperatures is shown in Fig. 14, hence the values obtained for dispersion parameters E_d , E_0 , and $n(0)$ for as prepared and annealed thin film samples were determined and listed in Table 5.

Fig. 15 shows the values of absorption coefficient (α) for the as-deposited and annealed $Se_{76}Te_{20}Sb_4$ films. It is clear that the absorption edge ($\alpha \geq 10^4$) shifts towards the high photon energy with increasing the annealing temperature that is related to the increasing of the optical band gap. It is convenient now to calculate the extinction coefficient from the values of λ and α using the formula $k = \alpha\lambda/4\pi$. Fig. 16 illustrates the dependence of k on the wavelength for different thin annealing temperature in crystallization region according to DSC curve.

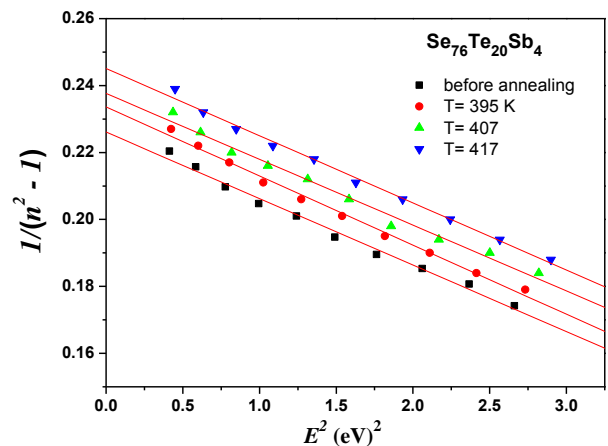


Fig. 14. Plot of refractive index factor $(n^2-1)^{-1}$ versus E^2 for as deposited and annealed $Se_{76}Te_{20}Sb_4$ films at 395, 407 and 417 K.

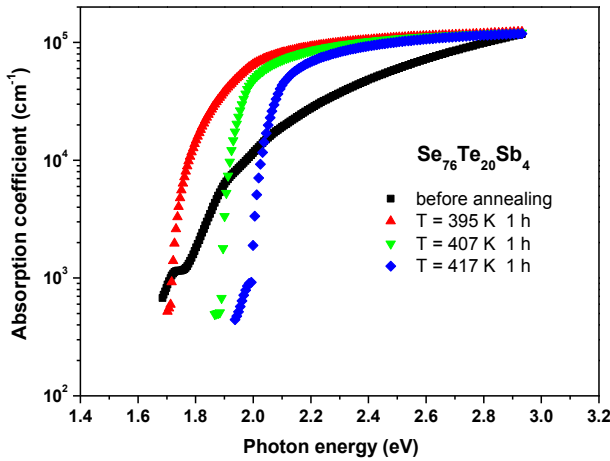


Fig. 15. The absorption coefficient α versus photon energy $h\nu$ for as deposited and annealed $Se_{76}Te_{20}Sb_4$ films at 395, 407, and 417 K.

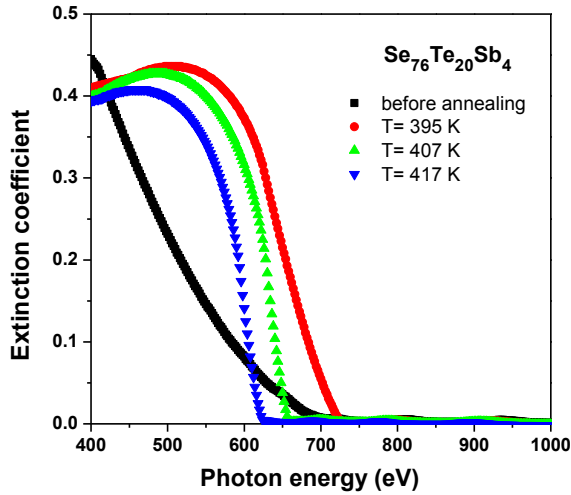


Fig. 16. The extinction coefficient, k versus photon energy, $h\nu$ for of the as prepared and annealed $Se_{76}Te_{20}Sb_4$ films at various temperatures (395, 407 and 417 K).

The possible optical transition of the annealed $Se_{76}Te_{20}Sb_4$ films were obeyed the allowed direct transition giving by the relation [34]:

$$\alpha(h\nu) = \frac{K(h\nu - E_g^{opt})^{1/2}}{h\nu} \quad (15)$$

while the possible optical transition of the as prepared $Se_{76}Te_{20}Sb_4$ films were obeyed the allowed non-direct transition (as demonstrated above)

Fig. 17 shows a good fitting of $(\alpha h\nu)^2$ versus photon energy ($h\nu$) for the annealed thin films, while shows a good fitting of $(\alpha h\nu)^{1/2}$ versus photon energy ($h\nu$) for the as prepared thin films. The values of the optical band gaps E_g^{opt} for the annealed and as prepared thin films were taken as the intercept of $(\alpha h\nu)^2$ versus $(h\nu)$ at $(\alpha h\nu)^2 = 0$

and the intercept of $(\alpha h\nu)^{1/2}$ versus $(h\nu)$ at $(\alpha h\nu)^{1/2} = 0$ respectively, then listed as shown in Table 5. The observed increase in the optical band gap with increasing annealing temperature may be due to the increase in grain size, the reduction in the disorder and decrease in density of defect states [35, 36] (which results in the reduction of tailing of bands) (the same reason that have mentioned above of decreasing the refractive index with increasing the annealing temperature). The increase of band gap with increasing annealing temperature is attributed to the amorphous–crystalline transformations.

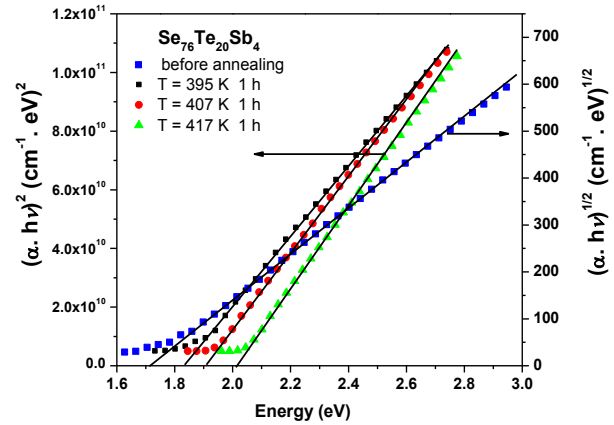


Fig. 17. The dependence of $(\alpha h\nu)^2$ on photon energy $h\nu$ for as prepared and annealed $Se_{76}Te_{20}Sb_4$ films at various temperatures (395, 407 and 417 K), from which the optical band gap E_g^{opt} is estimated (Tauc's extrapolation).

5. Conclusions

The optical constant (refractive index, extinction coefficient and absorption coefficient) of different composition and annealed films have been studied as a function of photon energy in the wavelength range 400 - 2500 nm. X-ray diffraction has been used to examine the structures of the as deposited and annealed films of these samples. Swanepoel method has been introduced to find the film thickness, refractive index, and hence other optical constants. It was found that the refractive index increases with increasing Sb content, which is related to the increased polarizability of the larger Sb atoms, in comparison with Se atoms. The optical band gaps of different compositions and annealed films can be determined in the strong absorption region and satisfied indirect transition for amorphous thin film and direct transition for annealed crystalline thin film. The increasing of Sb contents in the Se-Te glass system leads to increase in refractive index and decrease in the energy gap. This trend was discussed in terms of chemical bond approach of the elements involved. In an opposite behaviour the refractive index decrease while the energy gap increased with increasing the annealing temperature, related to the reduction of structural disorder present in these glassy thin

films. These properties may consider these materials suitable for optical data storage.

Acknowledgment

The authors are grateful to Al Azhar university-Faculty of Science Physics department Assuit branch, for financial support. Aswan university Faculty of Science-Physics department is also acknowledged.

References

- [1] K. Tanaka, K. Shimakawa, Amorphous Chalcogenide Semiconductors and Related Materials, DOI 10.1007/978-1-4419-9510-0_7, © Springer Science + Business Media, LLC 2011.
- [2] N. Suri, K. S. Bindra, P. Kumar, R. Thangaraj, J. Non-Cryst. Solids **353**, 1264 (2007).
- [3] E. R. Shaaban, Philos Mag. **88**, 781 (2008).
- [4] A. Dahshan, H. H. Amer, A. H. Moharram, A. A. Othman, Thin Solid Films **513**, 369 (2006).
- [5] E. R. Shaaban, M. A. Kaid, E. S. Moustafa, A. Adel, J. Phys. D: Appl. Phys. **41**, 125301 (2008).
- [6] E. R. Shaaban, Ishu Kansal, M. Shapaan, José M. F. Ferreira, J. of thermal analysis and calorimetry **98**, 347 (2009).
- [7] P. Kumar, T. S. Sathiaraj, R. Thangaraj, Phil. Mag. Lett **90**, 183 (2010).
- [8] S. A. Saleh, A. Al-Hajry, H. M. Ali, Phys. Scr. **84**, 015604 (2011).
- [9] P. Agarwal, S. Goel, J. S. P. Rai, A. Kumar, Phys. Stat. Sol. A **127**, 363 (1991).
- [10] O. El-Shazly, H. M. Khalifa, A. Sweyllam, F. F. El-Sanabary, E. F. El-Wahidy, Canadian Journal of Physics **92**(4), 328 (2014).
- [11] J. M. del Pozo, M. P. Herrero, L. Diaz J Non-Cryst Solids **185**, 183 (1995).
- [12] T. Rajagopalen, G. B. Reddy, Thin Solid Films **353**, 254 (1999).
- [13] J. M. del Pozo, L. Diaz, J Non-Cryst Solids **243**, 45 (1999).
- [14] Shamshad A. Khan, J. K. Lal, A. A. Al-Ghamdi, Optics & Laser Technology **42**, 839 (2010).
- [15] R. Swanepoel J. Phys. E: sci. Instrum. **16**, 1214 (1983).
- [16] J. C. Manifacier, J. Gasiot, J. P. Fillard J. Phys. E. **9**, 1002 (1976).
- [17] F. A. Jenkins, H. E. White, Fundamentals of Optics, McGraw-Hill, New York, 1957.
- [18] S. H. Wemple, DiDomenico Phys. Rev. B **3**, 1338 (1971).
- [19] K. Tanaka Thin Solid Films **66**, 271 (1980).
- [20] M. Krbal, T. Wagner, Mil. Vlcek, Mir. Vlcek, M. Frumar J. Non-Cryst. Solids **352**, 2662 (2006).
- [21] A. F. Loffe, A. R. Regel Prog. Semicond. **4**, 239 (1960).
- [22] A. H. Ammar, A. M. Farid, S. S. Fouad Physica B **307**, 64 (2001).
- [23] R. Valalova, L. Tichy, M. Vlcek, H. Ticha Phys. Status Solidi (a) **181**, 199 (2000).
- [24] J. Tauc (1974) Amorphous and Liquid Semiconductor (New York: Plenum).
- [25] F. Urbach Phys. Rev. B **92**, 1324 (1953).
- [26] E. R. Shaaban, Ishu Kansal, José M. F. Ferreira Physica B: Condensed Matter **404**, 3571 (2009).
- [27] V. Sadgopam, H. C. Gotos, Solid State Electron **8**, 529 (1965).
- [28] E. Mytilineou, J. Optoelectron. Adv. Mater. **4**, 705 (2002).
- [29] E. R. Shaaban, I. S. Yahia, M. Fadel, Journal of Alloys and Compounds, **469**, 427 (2009).
- [30] S. S. Fouad, A. H Ammar, M. Abo-Ghazala, Physica B **229**, 249 (1997).
- [31] E. A Davis, N. F. Mott Phil. Mag. **22**, 903 (1970).
- [32] Meherun-Nessa, K. Shimakawa, A. Ganjoo, J. Singh, J. Optoelectron. Adv. Mater. **2**, 133 (2002).
- [33] A. S. Soltan, A. A Abu-Sehly, M. A Abdel-rahim, J phys. & chem.. of solids **63**, 801 (2002).
- [34] J. Tauc, editor. Amorphous and liquid semiconductors. New York: Plenum Press; 1979. p. 159.
- [35] M. Ilyas, M. Zulfequar, M. Husain, J Mod Opt **47**, 663 (2000).
- [36] S. Shukla, S. Kumar J. Optoelectron. Adv. Mater. **12**, 1696 (2010).

*Corresponding author: esam_ramadan2008@yahoo.com